Nonequilibrium Monte Carlo simulation for a driven Brownian particle

Phil Attard
School of Chemistry F11, University of Sydney, New South Wales 2006, Australia
(Received 14 July 2009; revised manuscript received 5 September 2009; published 23 October 2009)

The author's nonequilibrium probability distribution is tested for time-varying mechanical work. Nonequilibrium Monte Carlo (NEMC) is used to simulate a Brownian particle in a soft-sphere solvent, driven by a moving external potential. Results are obtained for the phase lag and amplitude for drive frequencies ranging from the steady state to the transient regime. This now extends the application of the NEMC algorithm to a time-varying nonequilibrium system. The results are shown to agree with those obtained by nonequilibrium stochastic molecular dynamics and by Nosé-Hoover molecular dynamics, from which it is concluded that the nonequilibrium probability distribution correctly describes time-varying mechanical work and that it provides a fundamental basis for nonequilibrium statistical mechanics.

DOI: 10.1103/PhysRevE.80.041126 PACS number(s): 05.70.Ln, 05.20.−y, 05.40.Jc, 05.10.Ln

I. INTRODUCTION

The Boltzmann distribution for the phase-space probability is the foundation upon which classical equilibrium statistical mechanics is erected. In contrast, there is no consensus for the form of the probability distribution for nonequilibrium systems, and, consequently, there is currently no recognized foundation upon which to formulate a general theory for nonequilibrium statistical mechanics.

Many workers, implicitly or explicitly, invoke the equilibrium Boltzmann distribution for nonequilibrium systems. But this is readily demonstrated to be incorrect because the Boltzmann distribution is a function of the square of the molecular velocities and as such it is insensitive to the direction of time. The correct nonequilibrium probability distribution should depend upon the arrow of time, as mandated by the second law of thermodynamics.

At least two candidates for the nonequilibrium probability distribution that do depend upon the direction of time have been proposed. One due to Yamada and Kawasaki [1,2], and others [3,4], invokes the equilibrium Boltzmann distribution evaluated at some time in the past on an adiabatic trajectory from the present point in phase space. This would be appropriate for a subsystem originally in thermal equilibrium but subsequently isolated from the heat reservoir during the performance of the work or the application of the time-varying potential. Unfortunately, this is not the case for real nonequilibrium systems. Further, the Yamada-Kawasaki distribution cannot be generalized to steady-state thermodynamic systems such as heat flow. Finally, computer simulations, evaluating the past trajectory with and without a thermostat, have shown the Yamada-Kawasaki distribution to be intractable [5–8].

The second candidate for the nonequilibrium probability distribution is the one proposed by the present author [9,10]. This, like the equilibrium Boltzmann distribution, is simply the exponential of the reservoir entropy [11]. Unlike the equilibrium case, the latter is not determined solely from the current point in phase space but requires the calculation of the previous history of the nonequilibrium system up to the present time, which is where the arrow of time enters. As discussed further below, this can be cast in a form tractable for computation and for mathematical analysis. Although this nonequilibrium probability distribution has been successfully tested for steady heat flow [9], it has yet to gain wide-spread acceptance. Conceivably, there might be something special about the steady-state limit, and a more stringent test is called for. Time-varying work, for example, would go beyond those zero-frequency results and would provide a convincing demonstration of the general solution to the nonequilibrium problem.

The motivation for the present paper is to show that a closed-form expression for the nonequilibrium probability distribution does indeed exist and to test it in the case of a time-varying externally applied potential. This extends the earlier tests for a steady thermodynamic gradient [9] to a new time regime and to a qualitatively different nonequilibrium system, namely, a time-varying mechanical potential. The success of the theory in this case would extend the regime of validity beyond the steady-state regime and beyond the thermodynamic regime, and it would provide one with increased confidence in the generality of the approach.

The nonequilibrium probability distribution is here tested using nonequilibrium Monte Carlo (NEMC) simulations [9]. Given the increasing importance of computer simulation techniques in modern statistical mechanics [11,12], new algorithms are important in their own right. To date nonequilibrium simulations have been dominated by molecular dynamics (MD), either deterministic [8,12] or stochastic (SMD) [13]. The latter, which is derived by maximizing the second entropy that appears in the transition probability [10,14], has been applied to two nonequilibrium cases, namely, steady heat flow and time-varying mechanical work [10,13]. The development of a Monte Carlo algorithm for nonequilibrium systems provides an alternative to the molecular-dynamics approaches. In principle, Monte Carlo techniques offer advantages in complex systems with slow dynamics due to the inherent mathematical flexibility and potential for optimization that comes from sampling a probability distribution [11].

The present paper uses NEMC to directly test the nonequilibrium probability distribution for a mechanical transient case. Simulations are performed for a Brownian particle in a solvent bath and trapped by an externally applied potential, whose position varies harmonically with time. NEMC

results for the amplitude and phase lag of the driven particle are shown to be in quantitative agreement with results obtained using the nonequilibrium SMD algorithm [13] and MD results with a Nosé-Hoover chain thermostat [15]. The agreement between all three methods proves the author's nonequilibrium probability distribution for time-varying systems.

Some may be skeptical that it is possible to use Monte Carlo to describe a nonequilibrium system. There are two points to make. First, it is shown below that the present nonequilibrium Monte Carlo results are in quantitative agreement with those obtained by two established molecular-dynamics algorithms. So one can be assured that nonequilibrium Monte Carlo does work, even if one cannot at this stage appreciate how it is possible. Second, the reason for skepticism about nonequilibrium Monte Carlo could quite rightly concern the arrow of time and how this can possibly be part of a Monte Carlo algorithm since points in phase space can have no instantaneous knowledge of the second law of thermodynamics. As is shown with mathematical precision below, for each sampled point in phase space two trajectories over time are generated, and this is where the arrow of time enters the algorithm. Of course, it is not at all obvious how one might cast such an idea in a computationally tractable form, but one of the benefits of having a complete nonequilibrium theory is that it provides a framework to do just that.

II. PROBABILITY DENSITY

In the present author's theory for nonequilibrium thermodynamics and statistical mechanics, the nonequilibrium probability density in the subsystem phase space is the exponential of the reservoir entropy [9,10]

$$\wp(\mathbf{\Gamma},t) = e^{S_{\rm r}(\mathbf{\Gamma},t)/k_{\rm B}}/Z(t). \tag{2.1}$$

Here $\mathbf{\Gamma} \equiv \{\mathbf{q}^N, \mathbf{p}^N\}$ is a point in the subsystem phase space, t is time, $Z(t)$ is the partition function, which normalizes the integral of the probability density to unity, and $k_{\rm B}$ is the Boltzmann constant. This result follows from the fact that a point in the subsystem phase has no internal entropy [11]. The subsystem is connected to a thermal reservoir, whose entropy comprises an equilibrium and a nonequilibrium part [10],

$$S_{\rm r}(\mathbf{\Gamma},t) = S_{\rm eq}(\mathbf{\Gamma},t) + S_{\rm ne}(\mathbf{\Gamma},t). \tag{2.2}$$

The equilibrium part is that part of the reservoir entropy that would exist if the system had no memory. In the present case of a mechanical nonequilibrium system in contact with a thermal reservoir of temperature T, the subsystem Hamiltonian has an explicit time dependence $\mathcal{H}(\mathbf{\Gamma},t)$, and the equilibrium part of the reservoir entropy is

$$S_{\rm eq}(\mathbf{\Gamma},t)/k_{\rm B} = -\beta\mathcal{H}(\mathbf{\Gamma},t), \tag{2.3}$$

where $\beta \equiv 1/k_{\rm B}T$. In general, the equilibrium part of the reservoir entropy is insensitive to the direction of time,

$$S_{\rm eq}(\mathbf{\Gamma}^\dagger,t) = S_{\rm eq}(\mathbf{\Gamma},t), \tag{2.4}$$

where the conjugate phase-space point has the momenta reversed $\mathbf{\Gamma}^\dagger \equiv \{\mathbf{q}^N, (-\mathbf{p})^N\}$. For the potential trap used in the present simulations, with minimum located at $b(t)\hat{\boldsymbol{x}}$, there is also a spatial symmetry involving reflection of the solute and solvent coordinates in the trap minimum. Defining $\mathbf{\Gamma}^\ddagger \equiv \{(b(t)\hat{\boldsymbol{x}} - \mathbf{q})^N, \mathbf{p}^N\}$, one has as well

$$S_{\rm eq}(\mathbf{\Gamma}^\ddagger,t) = S_{\rm eq}(\mathbf{\Gamma},t). \tag{2.5}$$

This spatial symmetry operation is required below (see also Sec. 5D2 of Ref. [10]).

The nonequilibrium part of the reservoir entropy removes the adiabatic contribution from the change in the equilibrium part of the reservoir entropy [10],

$$S_{\rm ne}(\mathbf{\Gamma},t) = -\int_{t_0}^{t} dt' \dot{S}^0_{\rm eq}(\overline{\mathbf{\Gamma}}(t'|\mathbf{\Gamma},t),t'). \tag{2.6}$$

Here $\overline{\mathbf{\Gamma}}(t'|\mathbf{\Gamma},t)$ is the most likely trajectory proceeding backward in time from the current point in phase space [9,10,13]. Strictly speaking, the nonequilibrium part of the reservoir entropy is the sum over all possible trajectories to the present point. Hence, this expression approximates this by the largest term, which is the most likely trajectory and neglects the contribution of fluctuations about this trajectory. For a long enough trajectory, the two termini are uncorrelated and the nonequilibrium part of the reservoir entropy has at most a trivial dependence on t_0, and this may be replaced by $t-\tau$ for some $\tau > 0$ [9,10,13]. For the present case of mechanical work, since energy is conserved under Hamilton's equations of motion, the adiabatic derivative of the equilibrium part of the reservoir entropy is

$$\dot{S}^0_{\rm eq}(\mathbf{\Gamma},t) = \frac{-\partial\mathcal{H}(\mathbf{\Gamma},t)}{T\,\partial t}. \tag{2.7}$$

Only the time-dependent external potential contributes to this. Here T is temperature, which is the usual energy derivative of the first entropy. According to the present theory, temperature is well defined in all circumstances for equilibrium and nonequilibrium systems [10,11,16]. The superscript 0 denotes adiabatic here and throughout.

One now introduces three approximations [10]. First, all of the sensitivity of the nonequilibrium probability density to the arrow of time is contained the nonequilibrium part of the reservoir entropy, and so this may be approximated by its odd projection,

$$S_{\rm ne}(\mathbf{\Gamma},t) \approx S^{\rm odd}_{\rm ne}(\mathbf{\Gamma},t) = \frac{-1}{2}\int_{t-\tau}^{t} dt' [\dot{S}^0_{\rm eq}(\overline{\mathbf{\Gamma}}(t'|\mathbf{\Gamma},t),t') - \dot{S}^0_{\rm eq}(\overline{\mathbf{\Gamma}}(t'|\mathbf{\Gamma}^{\dagger\ddagger},t),t')]. \tag{2.8}$$

Note that both time and space symmetries are invoked in defining this odd function (see Sec. 5D2 of Ref. [10]). The twin justifications for this are that the even projection is negligible compared to the equilibrium part of the reservoir entropy and that this only differs from the true nonequilibrium part of the reservoir entropy on unlikely points of phase space, which occur with negligible probability in the thermodynamic limit [10]. At large times, the integrand goes to zero because the adiabatic rate of entropy production is indepen-

dent of the starting point of the trajectory [9,10],

$$\dot{S}^0_{\rm eq}(\overline{\mathbf{\Gamma}}(t'|\mathbf{\Gamma},t),t') \to \overline{\dot{S}^0_{\rm eq}}(t'), |t'-t| \to \infty. \tag{2.9}$$

This means that for large enough values of τ, the odd projection is insensitive to the value of τ, a point that will be tested by the simulation results below.

The second approximation is that the integrand is approximately an even function of time. This follows because a fluctuation in the most likely flux is as equally likely to be returning *to* the optimum state as it is to be coming *from* the optimum state. Hence, one has

$$S^{\rm odd}_{\rm ne}(\mathbf{\Gamma},t) \approx \frac{-1}{2}\int_t^{t+\tau} dt'[\dot{S}^0_{\rm eq}(\overline{\mathbf{\Gamma}}(t'|\mathbf{\Gamma},t),t') - \dot{S}^0_{\rm eq}(\overline{\mathbf{\Gamma}}(t'|\mathbf{\Gamma}^{\dagger\ddagger},t),t')]. \tag{2.10}$$

For this to be meaningful, for $t'>t$ one has to define a future Hamiltonian $\tilde{\mathcal{H}}(\mathbf{\Gamma},t';t)=\mathcal{H}(\mathbf{\Gamma},2t-t')$ and calculate the future most likely trajectory using it. This is required to avoid violating time causality: the future behavior can only be the same as in the past if the time variation in the external potential in the future is the reverse of what it was in the past.

Third, the future most likely trajectory is approximately equal to the future adiabatic trajectory, so that

$$S^{\rm odd}_{\rm ne}(\mathbf{\Gamma},t) \approx S^{\rm odd;0}_{\rm ne}(\mathbf{\Gamma},t) \equiv \frac{-1}{2}\int_t^{t+\tau} dt'[\dot{S}^0_{\rm eq}(\mathbf{\Gamma}^0(t'|\mathbf{\Gamma},t),t') - \dot{S}^0_{\rm eq}(\mathbf{\Gamma}^0(t'|\mathbf{\Gamma}^{\dagger\ddagger},t),t')]. \tag{2.11}$$

This is somewhat akin to Onsager's regression hypothesis that the subsidence of a fluctuation is the same in an isolated system as in one exchanging with a reservoir. This equality only holds in the future.

In view of the time reversibility of an adiabatic trajectory under Hamilton's equations, the definition of the future Hamiltonian means that one has exactly

$$\mathbf{\Gamma}^0(t'|\mathbf{\Gamma}^{\dagger\ddagger},t) = [\mathbf{\Gamma}^0(2t-t'|\mathbf{\Gamma},t)]^{\dagger\ddagger}. \tag{2.12}$$

[The double dagger means reflection in $b(t)\hat{\boldsymbol{x}}$ on the left-hand side, and in $b(2t-t')\hat{\boldsymbol{x}}$ on the right-hand side.] Because the motion of the external potential trap has been reversed for $t'>t$, it is necessary to both reverse velocities and to reflect the positions in the trap minimum. [For an adiabatic system with time-dependent potential, if $\mathbf{\Gamma}_2=\mathbf{\Gamma}^0(t_2|\mathbf{\Gamma}_1,t_1)$, then $\mathbf{\Gamma}_1=\mathbf{\Gamma}^0(t_1|\mathbf{\Gamma}_2,t_2)$, which is just a statement of the uniqueness of the trajectory. If one has a Hamiltonian that is not explicitly dependent on time $\mathcal{H}(\mathbf{\Gamma})$ then the reversibility of the equations of motion in addition implies $\mathbf{\Gamma}_1^\dagger=\mathbf{\Gamma}^0(2t_2-t_1|\mathbf{\Gamma}_2^\dagger,t_2)$. This last result does not hold for an explicitly time-dependent Hamiltonian, in which case it has to be replaced by Eq. (2.12).] Equation (2.12) allows the odd adiabatic nonequilibrium reservoir entropy to be rewritten exactly as

$$\begin{aligned} S^{\rm odd;0}_{\rm ne}(\mathbf{\Gamma},t) &= \frac{-1}{2}\int_{t-\tau}^{t} dt'[\dot{S}^0_{\rm eq}(\mathbf{\Gamma}^0(t'|\mathbf{\Gamma},t),t') - \dot{S}^0_{\rm eq}(\mathbf{\Gamma}^0(t'|\mathbf{\Gamma}^{\dagger\ddagger},t),t')] \\ &= \frac{1}{2T}\int_{t-\tau}^{t} dt'[\dot{\mathcal{H}}^0(\mathbf{\Gamma}^0(t'|\mathbf{\Gamma},t),t') - \dot{\mathcal{H}}^0(\mathbf{\Gamma}^0(t'|\mathbf{\Gamma}^{\dagger\ddagger},t),t')]. \end{aligned} \tag{2.13}$$

This uses the result that the adiabatic derivative satisfies $\dot{S}^0_{\rm eq}(\mathbf{\Gamma}^{\dagger\ddagger},t)=-\dot{S}^0_{\rm eq}(\mathbf{\Gamma},t)$. Of course, one can formally evaluate this integral because the integrand is an exact differential, but nothing is to be gained by this.

With these three steps, the nonequilibrium probability distribution becomes

$$\wp(\mathbf{\Gamma},t) = \frac{1}{Z(t)}e^{-\beta\mathcal{H}(\mathbf{\Gamma},t)}e^{S^{\rm odd;0}_{\rm ne}(\mathbf{\Gamma},t)/k_{\rm B}}. \tag{2.14}$$

The Monte Carlo simulations reported below calculate the nonequilibrium part of the reservoir entropy that appears here by calculating the two adiabatic trajectories backward in time and evaluating the integral with the trapezoidal rule or Simpson's rule. Using this probability density in the Monte Carlo simulations tests both the fundamental probability density and the three steps leading to the final form.

III. RESULTS FOR DRIVEN BROWNIAN MOTION

A. System details and Monte Carlo algorithm

A Brownian particle in a moving potential trap was simulated, using the same model treated in Refs. [13,15]. The subsystem consisted of a solute atom in a bath of $N=500-1000$ solvent atoms. The solute and solvent interacted via a soft-sphere potential,

$$u_{\alpha\gamma}(r) = [\sigma_{\alpha\gamma}/r]^{12}. \tag{3.1}$$

The solvent had a mass $m_1=1$, a length scale $\sigma_{11}=0.5$, and a potential cutoff of $R_{\rm cut;11}=1.2$. The solute had $m_0=10$, it interacted with the solvent via $\sigma_{10}=2.25$, and $R_{\rm cut;10}=5.2$. The temperature was 3 in these units. The potential trapping the solute was a harmonic potential along the x axis, oscillating along that axis,

$$U(x,t) = \kappa[x-b(t)]^2/2, \tag{3.2}$$

with $\kappa=16.81$, and $b(t)=B\cos\omega t$, with $B=0.2$, unless stated otherwise.

A bulk system was simulated with periodic boundary conditions. A cube of edge length 8.98 or 11.31 was used (for $N=500$ or 1000 solvent atoms, respectively) and the solvent density was 0.69. A spatial neighbor table with small cells of edge length ≈ 0.3 was used, which is about a factor of 3–10 more efficient than the conventional choice of neighbor cells of size equal to the cut-off radius [16].

In a given simulation the radial frequency ω was fixed. The Metropolis algorithm and umbrella sampling was used. The umbrella potential was based upon the equilibrium Boltzmann distribution (see below). The number of Monte Carlo cycles in each simulation was 500–1650.

A Monte Carlo cycle consisted of the following. First, a trial move for the position of each solvent atom, with the solute fixed at the origin. Each solvent was moved successively. Each trial move was accepted or rejected based upon the usual Metropolis criteria, using the solvent-solvent and solvent-solute potentials [11,12]. At this stage, the external potential does not enter. The step length was chosen to give an acceptance rate of about 50%. This was repeated 10–25 times, (i.e., 10–25 moves per solvent atom per cycle). Then the solvent velocities were randomly chosen from the Maxwell-Boltzmann distribution, which is a Gaussian of variance $\sqrt{k_BT/m_1}$. Next, the solute velocity was chosen from a Gaussian of variance $\sqrt{k_BT/m_0}$. Then for the solute position, the y and z coordinates were left unchanged at the origin, and the x coordinate was chosen from a Gaussian of variance $\sqrt{k_BT/\kappa}$. All the solvent x coordinates were shifted by this value of the solute x coordinate, so that their position relative to the solute remained unchanged. At this stage of the cycle, the procedure is equivalent to choosing the phase-space position of the solute and solvent from an equilibrium Boltzmann distribution with the external potential being located at the origin, (i.e., the position of the trap minimum being located at the origin). This phase-space coordinate (solute plus solvent) $\mathbf{\Gamma}_\alpha$, is stored, and after the following loop of trajectories and averages, it is used as the starting point for the next set of trial moves, by shifting the solute and solvent by the solute x coordinate to bring it back to the origin while maintaining the relative solvent positions.

Now a loop is performed over a set of 10 times, $t_1, t_2, \ldots$, typically evenly spaced on the interval $[0, 2\pi/\omega]$. Each time defines the location of the external potential $b_i = B\cos\omega t_i$. For each time, the solute and the solvent x coordinates are shifted by the amount b_i, so that their position relative to the trap is maintained. This phase-space coordinate may be denoted $\mathbf{\Gamma}_{\alpha,i}$. For each such coordinate, two adiabatic trajectories were calculated backward in time $\mathbf{\Gamma}^0(t'|\mathbf{\Gamma}_{\alpha,i}, t_i)$ and $\mathbf{\Gamma}^0(t'|\mathbf{\Gamma}^{\dagger\ddagger}_{\alpha,i}, t_i)$, for $t' \in [t_i, t_i - \tau]$. The maximum time interval was $\tau = 7$. The second-order Verlet algorithm [11,12] with a time step of 2×10^{-2} was used for the trajectory calculation. The time variation in the external potential was included in the calculation of the trajectories. A running integral of the partial time derivative of the external potential was performed over each trajectory, one was subtracted from the other, and $S^{\mathrm{odd};0}_{\mathrm{ne}}(\mathbf{\Gamma}_{\alpha,i}; t_i, \tau')$ was stored for 20 values of τ' uniformly spaced in the interval $[0, \tau]$.

After this loop averages were collected. Any given phase function $f(\mathbf{\Gamma}, t)$ has 200 distinct averages: one for each t_i, and one for each τ'. In view of the umbrella sampling (the umbrella weight is the equilibrium Boltzmann factor), an average value is

$$\langle f(t_i)\rangle_{\tau'} = \frac{\sum_\alpha f(\mathbf{\Gamma}_{\alpha,i}, t_i) e^{S^{\mathrm{odd};0}_{\mathrm{ne}}(\mathbf{\Gamma}_{\alpha,i}; t_i, \tau')/k_B}}{\sum_\alpha e^{S^{\mathrm{odd};0}_{\mathrm{ne}}(\mathbf{\Gamma}_{\alpha,i}; t_i, \tau')/k_B}}. \tag{3.3}$$

The two main quantities averaged in each simulation were the solute position $x(t)$ and the solute velocity $\dot{x}(t)$, and from them the amplitude and phase lag of the response from the functions $\langle x(t_i)\rangle_{\tau'} = A\cos(\omega t_i + \phi)$, $\langle \dot{x}(t_i)\rangle_{\tau'} = -A\omega\sin(\omega t_i + \phi)$. For each t_i and τ', these can be inverted to obtain the amplitude and phase lag $A_i = \sqrt{x_i^2 + \dot{x}_i^2/\omega^2}$ and $\phi_i = \tan^{-1}([\dot{x}_i + \omega x_i]/[\dot{x}_i - \omega x_i])$. Values of ϕ in the first quadrant were shifted to the third, so that $\phi \in [-\pi, 0]$. For each τ', these were simply averaged over the $10t_i$ to obtain the average amplitude and phase, $A_{\tau'}$, and $\phi_{\tau'}$, and an estimate in the standard error in the mean of this average. Statistical error creates problems with the phase lag for small values of the lag due to the branch cut. Hence, an alternative approach was also used, in which the two trigonmetric response functions were fitted in a least-squares sense to all the data at the $10t_i$ to obtain $A_{\tau'}$ and $\phi_{\tau'}$. Except for the smallest values of τ' (see discussion), the two methods gave very similar results.

Two minor modifications to the umbrella weight were explored. In the above procedure, the insensitivity of the Boltzmann distribution to the reflection operation $\mathcal{H}(\mathbf{\Gamma}^{\dagger\ddagger}, t) = \mathcal{H}(\mathbf{\Gamma}, t)$, and the definition of the odd projection $S^{\mathrm{odd};0}_{\mathrm{ne}}(\mathbf{\Gamma}; t, \tau) = -S^{\mathrm{odd};0}_{\mathrm{ne}}(\mathbf{\Gamma}^{\dagger\ddagger}; t, \tau)$ means that one can calculate the phase-space average for both $\mathbf{\Gamma}_{\alpha,i}$ and $\mathbf{\Gamma}^{\dagger\ddagger}_{\alpha,i}$ with no additional work (two configurations per t_i per cycle).

A second recipe for umbrella sampling was explored. In this case for each configuration α, a solute position $\tilde{x}_\alpha$ and velocity $\tilde{\dot{x}}_\alpha$ were chosen randomly from the Gaussians as above. A nominal amplitude $\tilde{A}$ and phase lag $\tilde{\phi}$ were fixed at the start of the simulation, and the actual position and velocity of the solute for configuration α and time t_i were taken as $x_{\alpha,i} = \tilde{x}_\alpha + \tilde{A}\sin(\omega t_i + \tilde{\phi})$ and $\dot{x}_{\alpha,i} = \tilde{\dot{x}}_\alpha + \tilde{A}\omega\cos(\omega t_i + \tilde{\phi})$. (It can be shown that the exact fluctuations about the most likely position and velocity in the nonequilibrium case are given by the above variances [10].) The weight used in the averages in this procedure is then

$$\frac{e^{-\beta\mathcal{H}(\mathbf{\Gamma}_{\alpha,i}, t_i)} e^{S^{\mathrm{odd};0}_{\mathrm{ne}}(\mathbf{\Gamma}_{\alpha,i}; t_i, \tau')}}{e^{-\beta\kappa\tilde{x}_\alpha^2/2} e^{-\beta m_0 \tilde{\dot{x}}_\alpha^2/2}}. \tag{3.4}$$

Only one configuration can be used at a time with this umbrella weight. The average amplitude and phase lag should be independent of the choice of $\tilde{A}$ and $\tilde{\phi}$, although one might expect the statistical error to be reduced by choices close to the final averages, and by reducing the width of the sampling.

B. Results

Figure 1 shows typical results of the nonequilibrium Monte Carlo simulation. The average position and velocity of the solute were obtained at ten different times in the drive cycle. The error bars are the standard error on the mean, which was obtained by breaking the simulation into in this case 25 blocks, and obtaining the variance of the averages. It can be seen that the data define quite well trigonometric curves, from which the phase lag and amplitude are readily extracted.

The data in Fig. 1 yielded $\langle A/B\rangle = 0.76 \pm 0.05$ and $\langle\phi\rangle = -1.31 \pm 0.05$. These data were obtained with umbrella sampling with $\tilde{A} = 0.66B$, and $\tilde{\phi} = -1.20$. Umbrella sampling instead with $\tilde{A} = 0.60B$, and $\tilde{\phi} = -1.00$ yielded $\langle A/B\rangle = 0.75 \pm 0.06$ and $\langle\phi\rangle = -1.14 \pm 0.11$. Using instead the Bolt-

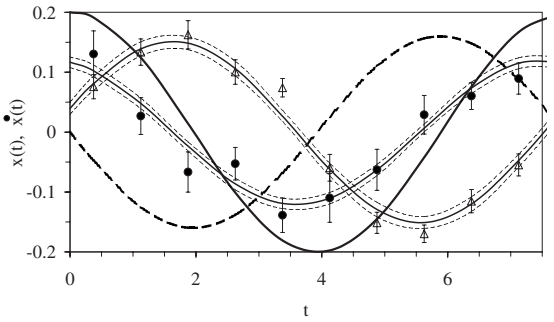

FIG. 1. Nonequilibrium Monte Carlo simulation results for the average position (open triangles) and velocity (filled circles) of the solute at 10 times t_i during the drive cycle ($\omega=0.8$, $B=0.2$, $\tau=7$). The solid curves are the trigonometric functions $x(t)=A\cos(\omega t+\phi)$ and $\dot{x}(t)=-A\omega\sin(\omega t+\phi)$, where A and ϕ are obtained from a simple average of the $10A[x(t_i),\dot{x}(t_i)]$ and $\phi[x(t_i),\dot{x}(t_i)]$. The enveloping dashed curves are a guide to the estimated error. The bold solid and dashed curves are the position $b(t)$ and velocity $\dot{b}(t)$ of the trap, respectively (dimensionless units here and throughout).

zmann distribution for the umbrella sampling yielded $\langle A/B\rangle=0.736\pm0.007$ and $\langle\phi\rangle=-1.23\pm0.01$, using 2.5 times the number of trajectories (effectively five times the number of configurations). One can conclude from this that the averages are independent of the umbrella weighting. The computational efficiency (i.e., number of trajectories required to obtain a specified statistical error) of the two types of umbrella weight tested here is slightly better for the Boltzmann weighting than for the Gaussian weighting.

It should be understood that if one had carried out ordinary equilibrium Monte Carlo on this system (i.e., sampled the Boltzmann distribution itself), then one would have obtained data scattered about the drive position itself (i.e., for the position, no phase lag and response amplitude equal to the drive amplitude, and an average velocity of zero). Of course, it is physically unreasonable to have a time-varying average position but a zero average velocity. This is just another way of saying that the Boltzmann distribution is not the correct probability distribution for a nonequilibrium system. The nonequilibrium part of the reservoir entropy in the present nonequilibrium probability distribution is an essential addition to the Boltzmann factor to produce a nontrivial response to the time-varying force.

The dependence of the nonequilibrium part of the reservoir entropy on the time interval used to calculate it is explored in Fig. 2. Here, the NEMC averages for the phase lag and for the amplitude ratio are plotted as a function of the time interval over which the trajectories were integrated to obtain the averages (i.e., $\langle\phi\rangle_{\tau'}$, and $\langle A/B\rangle_{\tau'}$). As the time interval is increased, the averages become constant. This is consistent with the claim made in the text that for large enough τ, the nonequilibrium part of the reservoir entropy is insensitive to the value of the time interval. In this case, the figure shows that the averages have reached their asymptotic values for $\tau'\gtrsim3$.

As $\tau'\to0$, the nonequilibrium part of the reservoir entropy vanishes. As discussed above, this limit is equivalent to using the Boltzmann distribution as the probability distribu-

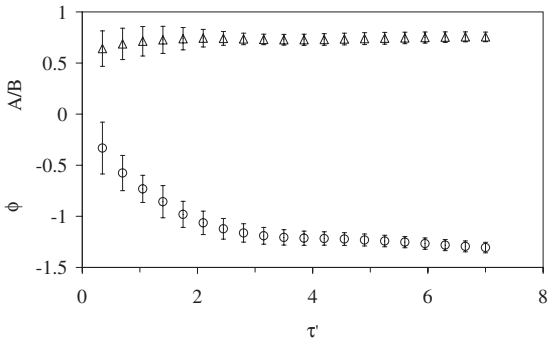

FIG. 2. Nonequilibrium Monte Carlo simulation results for the average relative amplitude $\langle A/B\rangle_{\tau'}$ (triangles) and phase lag $\langle\phi\rangle_{\tau'}$ (circles) of the solute as a function of the time interval τ' used for the averages ($\omega=0.8$, $B=0.2$).

tion, in which case one would obtain $\langle x(t)\rangle_{\rm eq}=B\cos\omega t$ and $\langle\dot{x}(t)\rangle_{\rm eq}=0$. The inconsistency of these two results from the fact that the Boltzmann distribution is inappropriate for a nonequilibrium system. The data in Fig. 2 at small τ are less reliable, in part because statistical noise makes estimates of ϕ for small ϕ problematic due to the branch cut, and in part because of this inconsistency in the fitted functions (i.e., fitting to position alone would give $A=B$ and fitting to velocity alone would give $A=0$). One can conclude from Fig. 2 that one should use a large enough value of τ for the data to have attained its asymptotic value. Recording averages as a function of τ in order to retrospectively confirm that the data have indeed reached their asymptotes creates no extra computation time because the umbrella weight can be saved as a running integral of τ'.

Figure 3 shows the phase lag of the solute as a function of the drive frequency. The solute oscillates almost in phase with the trap at low frequencies and increasingly lags the trap as the frequency is increased, going through $\phi=-\pi/2$ at approximately $\omega=1.3$. The results of the present NEMC algo-

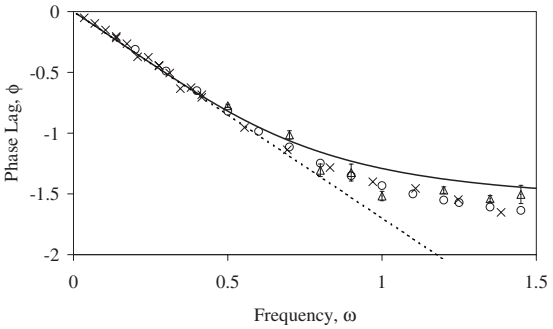

FIG. 3. Phase lag of the solute as a function of the drive frequency. The crosses are MD simulations with the equilibrium Nosé-Hoover chain thermostat [15], the circles are nonequilibrium stochastic molecular-dynamics simulations [13], and the triangles are the present nonequilibrium Monte Carlo simulations ($\tau'=7$). The dotted line is the Langevin steady-state theory ($D=0.105$, linear order in frequency), and the solid curve invokes the first non-Markov correction to the Langevin equation ($n=3$, $\tau=1$, quadratic order) [15]. The error bars are the standard error on the mean and are, in most cases, smaller than the symbols.

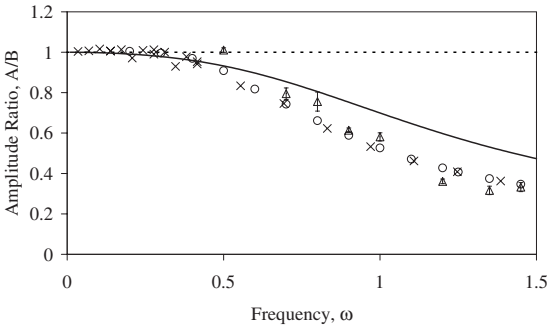

FIG. 4. Relative amplitude of the driven solute. Symbols and curves as in the preceding figure.

rithm are compared with conventional Nosé-Hoover simulations that employ a chain thermostat [15] and with the author's stochastic molecular-dynamics algorithm, which is based upon the second entropy for the transition probability [13]. All three simulation results are in good agreement, which supports the validity of all three. That the two molecular-dynamics algorithms agree is expected; as has been shown [10,13], the particular thermostat has negligible influence in the thermodynamic limit of the solvent for this type of mechanical work applied only to a single solute (see Secs. SSIII.B.7 and VI.C.3 of [10], and Sec. II.B.3 of [13]). However, the test of the NEMC is more significant as this is a qualitatively different approach to the molecular-dynamics approaches. It relies upon the correct weighting of phase space. The fact that the phase lag obtained in this approach is the same as that given by the molecular-dynamics simulations is strong evidence for the validity of the nonequilibrium probability distribution that is invoked. One can conclude that the NEMC algorithm and the underlying nonequilibrium probability distribution are valid over the whole temporal regime from steady state to transient.

The low-frequency data in Fig. 3 correspond approximately to the steady state. This regime is well described by the Langevin theory, and in it the particle moves with the instantaneous velocity of the trap $\dot{\bar{x}}(t)=\dot{b}(t)$ and lags the trap such that the drag force is equal and opposite to the trap force $-\beta\kappa[\bar{x}(t)-b(t)]=\dot{b}(t)/D$ [15]. In this case to the leading order in frequency, $A=B+\mathcal{O}(\omega^2)$ and $\phi=-\omega/\beta\kappa D+\mathcal{O}(\omega^3)$, with diffusion constant $D=0.105$ obtained from the position autocorrelation function in the absence of a trap [15]. (The most likely position and velocity given by this equation are self-consistent only to the leading order in frequency.) Also shown in Fig. 3 is the first-order correction to Langevin theory, which accounts for the leading memory effects in the solvent (i.e., essentially a time-dependent diffusion constant) [15]. It can be seen that this works well up to intermediate frequencies but underestimates the magnitude of the phase lag at higher frequencies. The high-frequency regime can be called the transient regime, and in this region there is a significant phase lag between the particle and the trap.

Figure 4 shows the ratio of the amplitude of the solute response to the amplitude of the driven trap. It can be seen that the response amplitude decreases with increasing frequencies. Again, there is good agreement between the three simulation methods.

There is some evidence for a weak nonlinear dependence of the amplitude response at higher drive amplitudes. For example, in the case of nonequilibrium SMD simulations, drive amplitudes of 5, 2.5, 1, and 0.5 give $\langle A/B\rangle=0.624\pm0.002$, 0.657 ± 0.002, 0.664 ± 0.005, and 0.675 ± 0.006, respectively. The NEMC simulations for drive amplitudes of 1, 0.5, and 0.2 give 0.68 ± 0.02, 0.78 ± 0.05, and 0.76 ± 0.05. The phase lag showed less variability with drive amplitude.

For the present case of a trapped Brownian solute, the nonequilibrium stochastic molecular-dynamics method is more efficient than the present implementation of the nonequilibrium Monte Carlo method. For example, at $\omega=0.8$, the SMD simulations used a total of 4×10^6 time steps to give $\langle A/B\rangle=0.675\pm0.006$ and $\langle\phi\rangle=-1.27\pm0.01$. The NEMC case at $\omega=0.8$ and for $\tau'=3$ used 625 trajectories, each of length 3000 times steps, a total of 1.9×10^6 time steps, giving $\langle A/B\rangle=0.73\pm0.05$ and $\langle\phi\rangle=-1.19\pm0.08$. (The data in Fig. 2 are for $\tau'=7$.) Hence, the error is reduced by about a factor of 10 for twice as many time steps, which means that SMD is about 50 times more efficient than NEMC in this case.

This inefficiency in the NEMC method is more apparent than real since no great effort was made to optimize the present version of the algorithm. It is clear that there is a great deal of redundancy in using 10 time nodes per cycle to get the amplitude and phase lag and that this number could be reduced; possibly, even a single node would be adequate, in which case the NEMC would be about four times more efficient than SMD if the error were unchanged. Also, in the second form of umbrella sampling about a specified amplitude $\tilde{A}$ and $\tilde{\phi}$, the variance used was the same as that expected for the fluctuations in the real system. There is no reason why the width of the umbrella sampling could not be reduced if the only quantity of interest is the averages themselves. In more challenging nonequilibrium cases, such as polymeric or glassy systems, the NEMC method offers much greater potential for optimization and for broad coverage of phase space than the SMD method. In any case, the main aim of the present paper was not so much to optimize the NEMC algorithm as it was to test the quantitative accuracy of the nonequilibrium probability distribution for a time-varying mechanical case.

IV. CONCLUSION

As mentioned in the introduction, the development of a general theory for nonequilibrium statistical mechanics is predicated upon an agreed upon form for the nonequilibrium probability distribution. This paper has tested the author's formulation of the problem for the case of a time-varying potential. A nonequilibrium Monte Carlo algorithm [9] was used to obtain phase-space averages with the nonequilibrium probability distribution. There was good agreement between the present results and results obtained with nonequilibrium stochastic molecular-dynamics [13] and with equilibrium chain Nosé-Hoover molecular-dynamics algorithms. Since the NEMC and the SMD approaches are qualitatively different, their agreement in this case augers well for the self-

consistency of the general nonequilibrium theory.

The author's nonequilibrium probability distribution has now been successfully tested for two cases: a steady-state thermodynamic case (steady heat flow) [9] and the present transient mechanical case (driven Brownian particle). These tests confirm that not only does a closed analytic form for the nonequilibrium probability distribution exist but also that the particular form obtained by the author is fundamentally sound and that it is applicable to the full spectrum of nonequilibrium systems.

[1] T. Yamada and K. Kawasaki, Prog. Theor. Phys. **38**, 1031 (1967).
[2] T. Yamada and K. Kawasaki, Prog. Theor. Phys. **53**, 111 (1975).
[3] L. P. Kadanoff and P. C. Martin, Ann. Phys. (N.Y.) **24**, 419 (1963).
[4] A. M. S. Tremblay, M. Arai, and E. D. Siggia, Phys. Rev. A **23**, 1451 (1981).
[5] G. P. Morriss and D. J. Evans, Mol. Phys. **54**, 629 (1985).
[6] B. L. Holian, W. G. Hoover, and H. A. Posch, Phys. Rev. Lett. **59**, 10 (1987).
[7] G. P. Morriss and D. J. Evans, Phys. Rev. A **37**, 3605 (1988).
[8] D. J. Evans and G. P. Morriss, *Statistical Mechanics of Nonequilibrium Liquids* (Academic Press, London, 1990).
[9] P. Attard, J. Chem. Phys. **124**, 224103 (2006).
[10] P. Attard, Annu. Rep. Prog. Chem., Sect. C: Phys. Chem. **105**, 63 (2009).
[11] P. Attard, *Thermodynamics and Statistical Mechanics: Equilibrium by Entropy Maximisation* (Academic Press, London, 2002).
[12] M. P. Allen and D. J. Tildesley, *Computer Simulation of Liquids* (Oxford University Press, Oxford, 1987).
[13] P. Attard, J. Chem. Phys. **130**, 194113 (2009).
[14] P. Attard, J. Chem. Phys. **122**, 154101 (2005).
[15] P. Attard and A. Gray-Weale, J. Chem. Phys. **128**, 114509 (2008).
[16] P. Attard, J. Chem. Phys. **121**, 7076 (2004).